Quantifying the effects of climate change on aircraft take-off performance at European airports

Williams, J. ORCID: https://orcid.org/0000-0002-0680-0098, Williams, P. D. ORCID: https://orcid.org/0000-0002-9713-9820, Guerrini, F. ORCID: https://orcid.org/0000-0003-1449-1587 and Venturini, M. ORCID: https://orcid.org/0009-0004-2881-1400 (2025) Quantifying the effects of climate change on aircraft take-off performance at European airports. Aerospace, 12 (3). 165. ISSN 2226-4310 doi: 10.3390/aerospace12030165 Available at https://centaur.reading.ac.uk/121638/

Published version at: http://dx.doi.org/10.3390/aerospace12030165
To link to this article DOI: http://dx.doi.org/10.3390/aerospace12030165

Publisher: MDPI

aerospace

MDPI

Article

Quantifying the Effects of Climate Change on Aircraft Take-Off Performance at European Airports

Jonny Williams [1,*], Paul D. Williams [1], Federica Guerrini [2] and Marco Venturini [2]

[1] Department of Meteorology, University of Reading, Reading RG6 6ET, UK
[2] Amigo s.r.l., 00196 Rome, Italy
* Correspondence: j.h.t.williams@reading.ac.uk

Abstract: This work uses state-of-the-art climate model data at 30 European airport locations to examine how climate change may affect summer take-off distance required—TODR—and maximum take-off mass—MTOM—for a 30-year period centred on 2050 compared to a historical baseline (1985–2014). The data presented here are for the Airbus A320; however, the methodology is generic and few changes are required in order to apply this methodology to a wide range of different fixed-wing aircraft. The climate models used are taken from the 6th Coupled Model Intercomparison Project (CMPI6) and span a range of climate sensitivity values; that is, the amount of warming they exhibit for a given increase in atmospheric greenhouse gas concentrations. Using a Newtonian force-balance model, we show that 30-year average values of TODR may increase by around 50–100 m, albeit with significant day-to-day variability. The changing probability distributions are quantified using kernel density estimation and an illustration is provided showing how changes to future daily maximum temperature extremes may affect the distributions of TODR going forward. Furthermore, it is projected that the 99th percentile of the historical distributions of TODR may by exceeded up to half the time in the summer months for some airports. Some of the sites studied have runways that are shorter than the distance required for a fully laden take-off, which means they must reduce their payloads as temperatures and air pressures change. We find that, relative to historical mean values, take-off payloads may need to be reduced by the equivalent of approximately 10 passengers per flight, as these significant increases (as high as approximately 60%) show a probability of exceeding historical extreme values.

Keywords: take-off distance; climate change; take-off mass; Europe; scenario

Academic Editor: Michael Schultz

Received: 19 December 2024
Revised: 24 January 2025
Accepted: 18 February 2025
Published: 20 February 2025

Citation: Williams, J.; Williams, P.D.; Guerrini, F.; Venturini, M. Quantifying the Effects of Climate Change on Aircraft Take-Off Performance at European Airports. *Aerospace* **2024**, *12*, 165. https://doi.org/10.3390/aerospace12030165

1. Introduction

Aircraft take-off distance required (TODR) and maximum take-off mass (MTOM) are critical parameters that must be considered for the safe operation of each and every military, civilian, and freight air movement. A 2016 order-of-magnitude estimate from the World Economic Forum put the total number of flights per day at approximately 10^5 globally [1]. Going forward, for Europe specifically, the European Organisation for the Safety of Air Navigation (EUROCONTROL) predicts an increase of between 19% and 76% in flight numbers between 2019 and 2050 [2].

Tables of TODR versus weight are typically publicly available for passenger aircraft up to the relevant maximum payload. For many large airports—e.g., Amsterdam Schiphol and London Heathrow—available runway lengths are more than capable of accommodating a fully laden Airbus A320, often with kilometres to spare. However, for airports with

runway lengths roughly equal to or shorter than the manufacturers' limits (or where the effective runway length is reduced due to maintenance or a take-off starting before the end of the runway), the weight of the aircraft must be reduced in order to comply with safety constraints.

For a given air pressure and aircraft mass, higher temperatures (e.g., due to climate change, as discussed in detail for nine European airport sites by Gallardo et al. [3]) reduce air density, which must be balanced by an increase in speed to achieve the same amount of lift to overcome gravity. Changes in density also affect aerodynamic drag, and hence the vertical and horizontal balances of forces are subject to change. Because of this, a given aircraft configuration in a warmer world will require a longer distance before take-off occurs and—equivalently—if there is a limited take-off distance (i.e., a particular runway), the maximum aircraft mass must be reduced.

This study builds on previous work that detailed the effects of past climate change on several Greek airports, taking (daily minimum) temperature and headwind speed into account [4]. This study found that maximum take-off weight is already affected by the changing climate and quantified this effect in terms of reduced passenger numbers and fuel payload for the Airbus A320 turbofan (using a model that the present study uses as its basis) and DHC-8-400 turboprop aircraft (using manufacturer data).

Other previous relevant studies include those of Coffel et al. and Wang et al. [5–7]. The former both consider a selection of airports in the USA, which were chosen for their high temperatures (Phoenix), elevation (Denver), or short runways (LaGuardia and Washington, DC). The former study used the most extreme emissions scenario available at the time (RCP8.5) and the latter used a more nuanced approach by also considering a more optimistic (lower emissions) RCP4.5 future. These studies differ subtly trom the study of Gratton et al. [4] in their concentration on 'weight-restriction days'; that is, the number (or fraction) of days in a particular time window when weight restrictions must be applied. The latter study of Wang et al. [7] studies the take-off performance of the Boeing 737 at four Asian airports (also under RCP8.5) and shows non-linear increases in TODR with temperature, resulting in increases of ≈100–200 m by the 2070s.

In this work, we combine the main analysis methods of the above studies using a Newtonian force-balance model and open-access input data to obtain estimates for how TODR and MTOM may change in the future using data from 10 state-of-the-art climate models and three future emissions scenarios. We consider 30 specific European airports using 1985–2014 as a recent historical baseline and 2035–2064 as our future period of interest. The use of simulated data over the historical period, rather than observations, enables the removal of any model-data biases, since these will be common to both the past and future periods chosen.

The structure of this paper is as follows: input climate model data and the force balance model are described in Section 2.1, the numerical methods are detailed in Section 2.2 and Section 2.3, respectively, results are given in Section 3, and we provide conclusions and suggestions for further work in Section 4.

2. Materials and Methods

2.1. Input Data

We use the method of Gratton et al. [4] to calculate take-off distances as a function of daily mean air pressure and daily maximum temperature at 2 m above ground level. The data used are from 10 climate models from the 6th Coupled Model Intercomparison Project ('CMIP6') and cover the 'historical' period 1985–2014 and projections for 2035–2064 for three different future climate scenarios. The historical simulations finish at the end of

2014 because the relevant forcing data for the simulations were not available after this date, when the models themselves were run. The models used are listed in Table A3.

These scenarios—or Shared Socieconomic Pathways (SSPs)—are described by two numbers; the first indicates the scenario 'family' that they belong to and the second provides the top-of-atmosphere radiative forcing in Watts per metre squared at 2100. We use the scenarios described in Table 1, which broadly correspond to low, medium, and high levels of future climate change.

Table 1. Description of climate change scenarios used in this work (see, e.g., [8]).

Title 1	Title 2
SSP1-2.6	Sustainable development [9]
SSP3-7.0	Regional rivalry [10]
SSP5-8.5	Fossil-fuelled development [11]

The data used are for the 25 busiest European airports—according to the 2019 European Civil Aviation Council data [12]—plus an additional five sites that (according to media reports) have already experienced either frequent noise complaints or take-off restriction issues related to short runways. Indeed, noise complaints are likely to increase in the future if increased take-off thrusts are required for runway length-limited airports. The study site ensemble is shown in Figure 1.

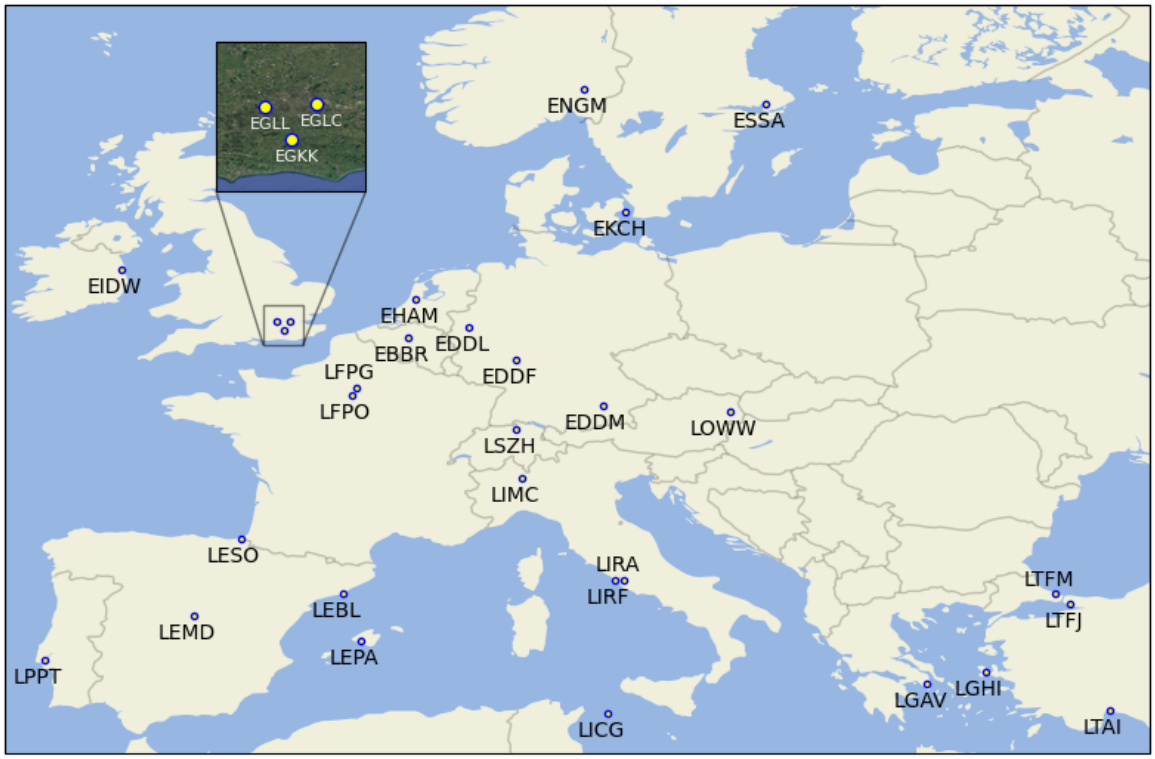

Figure 1. The 30 airports considered in this work. See Tables A1 and A2 for more information.

The climate model data used in this study are the surface air pressure, P_{surf} and the standard measure of 'Maximum temperature at 2 metres in the last 24 h', or T_{mx2t24} (e.g., https://codes.ecmwf.int/grib/param-db/51 accessed on 2 December 2024). Other variables were also extracted from the climate model data, including specific humidity—which affects sound propagation and hence noise pollution [13]—and will be used in future

work. The daily maximum temperature was chosen in order to enhance the signal-to-noise ratio in data with large day-to-day variability.

The air density is calculated assuming ideal gas conditions:

$$\rho = \frac{P_{\text{surf}}}{R_{\text{specific}} T_{\text{mx2t24}}} \tag{1}$$

where ρ is the air density and R_{specific} is the specific gas constant for dry air, 287 J·kg^{-1}·K.

The methodology used to prepare the model data in the required format for this study is based on Trentini et al. [14], which uses bias correction tailored to extreme events in the ERA5 reanalysis after the resolution of the raw model data is increased from their native ∼1° to that of ERA5, 0.1°; see references in Table A3 for further information. In addition, the current study introduces a Quantile Delta Mapping step, which helps to maintain variations over longer periods Trentini et al. [15]. Any values more than three standard deviations from the mean in any of the distributions studied were discarded to reduce the impact of outliers emerging from the model ensemble.

2.2. Take-off Distance Calculation

We used a method based on that of Gratton et al. [4], assuming a flat runway (no incline) for the Airbus A320 aircraft using V2500-A1 turbofan engines manufactured by International Aero Engines; Figure 2 illustrates the direction of the forces and angles involved.

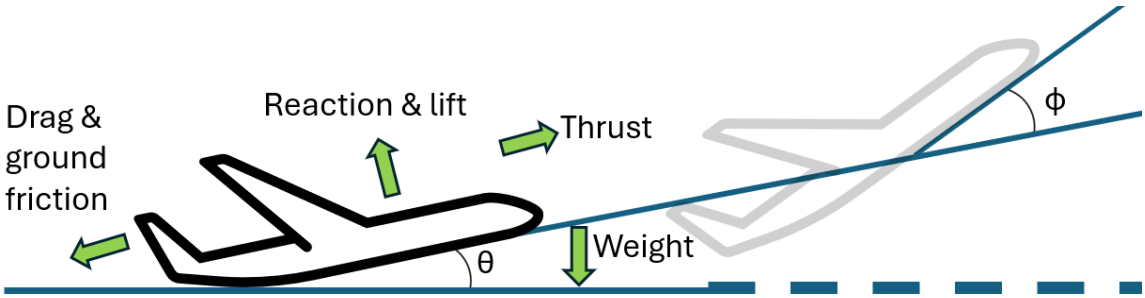

Figure 2. Angles and forces involved in TODR calculation; θ is the angle between the runway and the local horizontal plane and ϕ is the take-off angle between the flight path and the runway.

The forces on the aircraft were calculated assuming an altitude-dependent thrust—described in detail in Section 5.2.1 of [16]—and then the equations of motion were solved iteratively until the 'true air speed'—TAS—was found, where the lift is equal to the weight, i.e., the moment of take-off. The local wind speed is not taken into account in this calculation but could straightforwardly be included in the future. From this value of the take-off speed, and using the acceleration at each velocity, the amount of runway from rest to take-off is calculated. The TODR includes the horizontal distance from stand-still to take-off, plus the distance required to climb to 10.7 m (35 feet) above the runway, which is $\frac{10.7}{tan\phi} \approx 79$ m. Finally, the sum of these two distances is increased by a 15% safety margin [17] to give the final TODR. Thrust and drag data are obtained from the openAP package [16], where drag from landing gears is used but wave and wing flap drag are excluded. The openAP software (version 2.0) provides the minimum, optimum, and maximum values of take-off speeds (74.5, 85.3 and 96 m·s^{-1}) from the WRAP kinematic model of aircraft performance [18], and we use these values to find a corresponding lift coefficient (C_L) value envelope. By using the table of take-off distance as a function of mass from Gratton et al. [4], we find the lift coefficient via the minimisation of root–mean–square differences between model and manufacturer values:

1. Obtain the thrust value from the openAP model assuming minimum take-off speed.
2. Calculate the TODR as a function of the masses from Gratton et al. [4] for $C_L = 1$ to $C_L = 2$ in increments of 0.01.
3. Find the root–mean–squared difference (RMSD) value between the array of TODRs found in step 2 and the manufacturer values.
4. Find the value of C_L which gives the lowest RMSD value; this provides an estimate of the lower bound C_L,

$$\text{RMSD} = \sqrt{\overline{(\text{TODR} - \text{TODR}_{\text{manufacturer}})^2}} \tag{2}$$

5. Repeat steps 1–4 for the optimum and maximum take-off speeds. This will provide a central, optimum value of $C_{L,\text{opt}}$ with an associated uncertainty range.

The results of the above steps are shown in Figure 3 for ISA conditions and at mean sea level and show that the uncertainty considerations are valid in that they encompass the values from Gratton et al. [4] at every considered take-off mass, with the exception of the manufacturer's TODR value at the maximum take-off weight. This is where where one would expect this linear model to break down due to a lack of consideration of higher-order effects, which are outside the scope of this study [16,18]. Finally, we obtain the optimum value of the lift coefficient $C_{L,\text{opt}} = 1.14 \pm 0.03$.

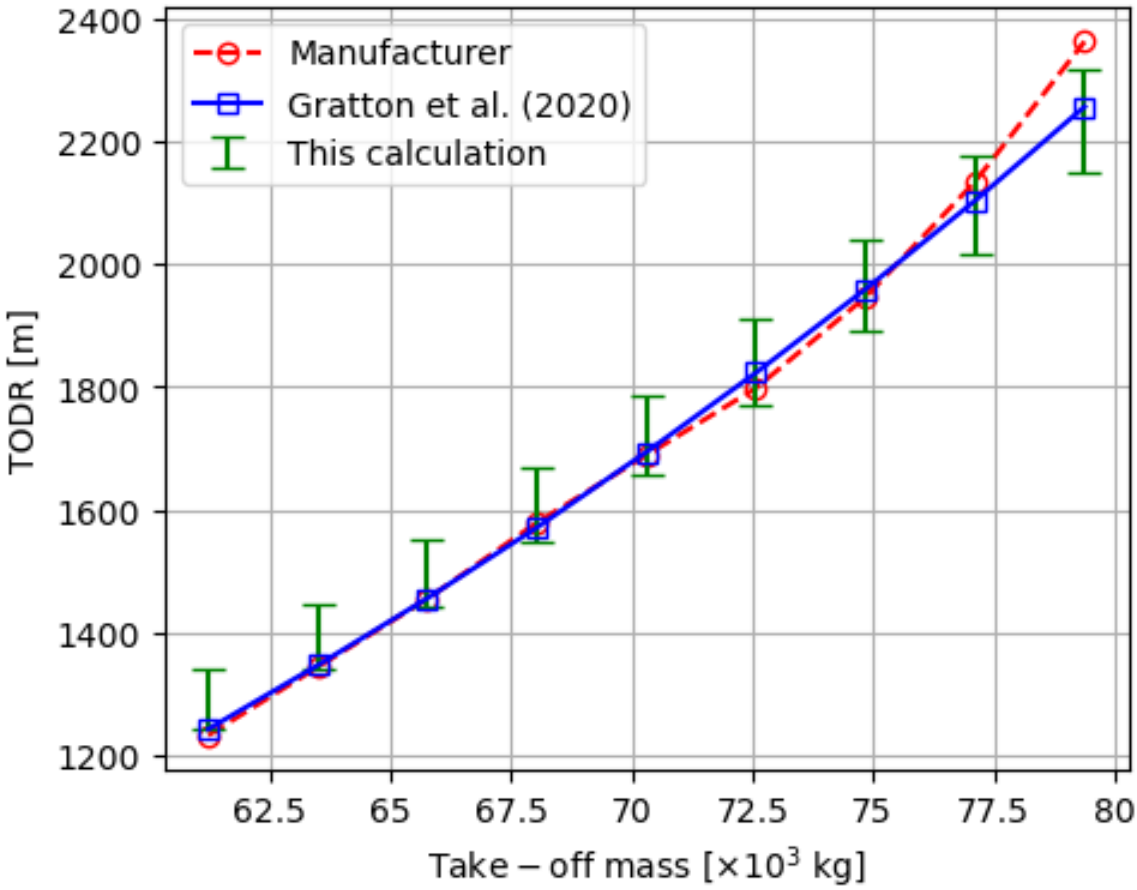

Figure 3. TODR as a function of mass for the Gratton et al. [4] study and for the the calculations presented here. Manufacturer values are also shown. Calculations were performed under ISA conditions and mean sea level. The numerical data from the open-access Gratton et al. study can be found in Table 1, Supplementary Material #2.

Since the calculation, as it stands, only uses air density as a thermodynamic input, we can straightforwardly find idealised (i.e., not using climate model data) TODR as a function of temperature and pressure independently by holding one constant and varying the other, since $\rho \sim \frac{P}{T}$. Example values are an increase of 4.2 m per degree and a decrease of 1.2 m per hPa at minimum payload (at maximum payload, the equivalent numbers are 7.4 m $\cdot$ K^{-1} and 2.2 m $\cdot$ hPa^{-1}) under International Standard atmosphere (ISA) conditions of 15 degrees Celsius and 1013.25 hPa.

2.3. MTOM Calculation

The algorithm and equations used here and in Gratton et al. [4] are, a priori, used to find the TODR for a given mass. To achieve the inverse of this—find the mass for a given TODR—the system must be inverted, and to achieve this we use a search algorithm that iteratively calculates TODR at decreasing values of take-off mass until the TODR is equal to the runway length. For every day of a model's time series, the TODR is calculated using the daily maximum temperature and surface pressure. We then follow the steps shown in the following pseudocode description (Figure 4).

```
→ if (TODR < runway length) then go to next day.
→ else
→ → Reduce mass by 10^3 kg until TODR < runway length.
→ → Add 10^3 to the mass.
→ → → Reduce mass by 10^2 kg until TODR < runway length.
→ → → Add 10^2 to the mass.
→ → → → Reduce mass by 10^1 kg until TODR < runway length.
→ → → → Add 10^1 to the mass.
→ → → → → Reduce mass by 10^0 kg until TODR < runway length.
→ → → → → Add 10^0 to the mass.
→ → → → → → Stop; MTOM has been found to the nearest kg.
```

Figure 4. Pseudocode description of the steps used to calculate the MTOM.

This allows us to efficiently find the mass that provides a TODR equal to the runway length to an accuracy of 1 m by minimising a function, f, of density ρ and altitude $\mathcal{H}$ (and potentially other variables, represented by the ellipsis, ...), in the following the form:

$$f(\rho, \mathcal{H}, \ldots) = \texttt{TODR}(\rho, \mathcal{H}, \ldots) - \texttt{runway length}, \tag{3}$$

This is faster than the 'brute force' method by over an order of magnitude. Other algorithms, such as the use of a binary search, could potentially obtain the findings of the MTOM even faster in the future. This would be of particular interest when considering longer periods and larger site ensembles.

Throughout this work, for illustrative purposes, we use the UKESM1-0-LL model as our input dataset and Heathrow airport for the site. All results are shown for June–July–August (JJA), and we split the results up into two main sections: the former looking at TODR and the latter at MTOM.

For TODR, we firstlexamined a specific model-airport case study for June–July–August (JJA) in order to illustrate the type of results available from the model at this stage. We used the UKESM1-0-LL model and London Heathrow airport—International Civil Aviation Organization code (ICAO) EGLL. We then examined all models and sites together, illustrating the variation across the entire ensemble of the probability of the future period exceeding 'one in a hundred days' warmth—and hence maximising the TODR.

For MTOM, we show results for four short-runway case study sites which are already runway-length limited (or, equivalently, requiring weight restrictions) for a fully-laden A320; Chios, Pantelleria, San Sebastian, and Rome Ciampino. As temperatures rise, these

weight-restrictions will become larger, assuming that engine thrust values are not altered, as was the case for the calculations performed here.

We did not include London City here since it does not operate the A320. All other airports in our study group have runways long enough to accommodate the A320 at maximum payload even under extreme warming conditions.

3. Results and Discussion

3.1. Take-Off Distance Required

3.1.1. Case Study

Figure 5 shows the distributions of TODR for the historical period and the three future forcing scenarios used for Heathrow airport in JJA using the UKESM1-0-LL climate model.

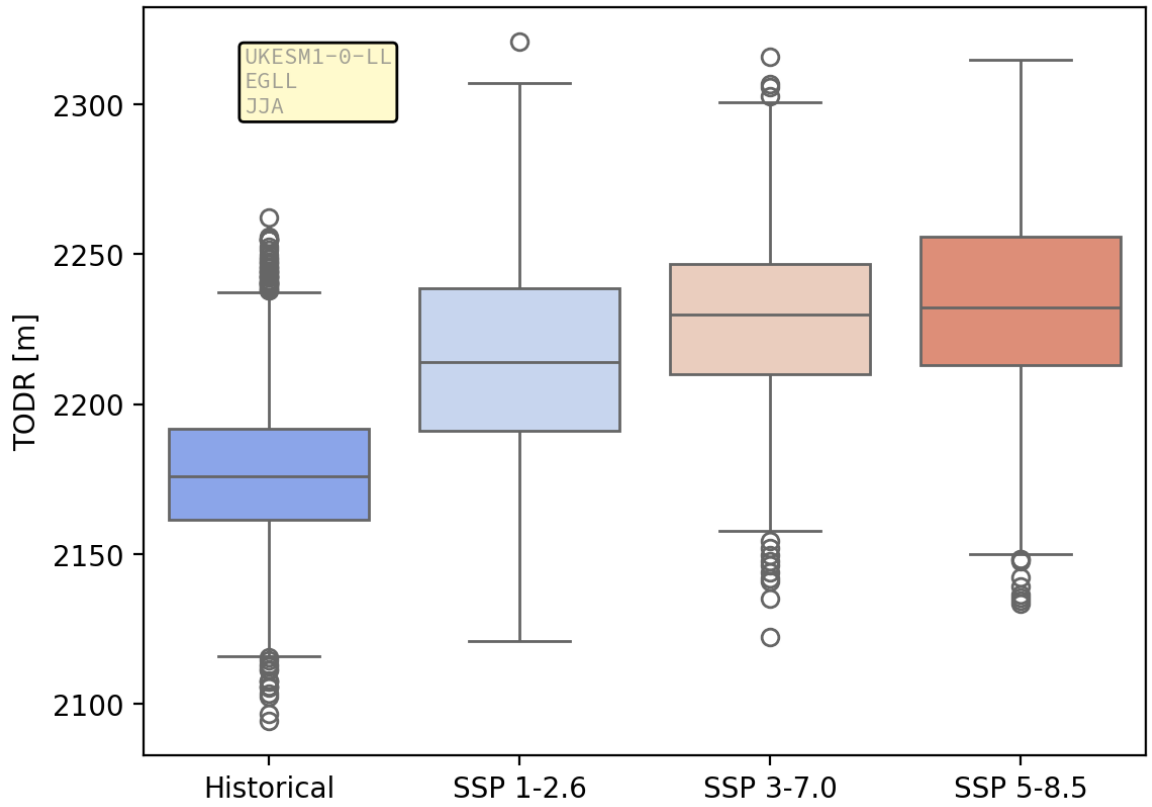

Figure 5. Distributions of TODR for Heathrow airport and UKESM1-0-LL in JJA for a fully laden A320 aircraft (78,000 kg). Data that are more than 1.5 times the inter-quartile range from the median are explicitly shown.

Figure 5 shows that, in general, the TODR increases with increased forcing. This is the expected first-order behaviour since warmer air will be less dense for a given air pressure, as shown in Equation (1). Note, however, that for some airport/model combinations, the median values of TODR do not always increase monotonically, as shown, for example, in Figure 6 for Brussels airport and the ACCESS-ESM1-5 model. This could be a function either of the chosen model's forcing response (in general or for this site specifically) or the bias correction pipeline, which was used to produce the data used in this modelling exercise [14]. In general, the behaviour of this, and related, quantities will always be model-dependent due to the differing values of climate sensitivity, process parameterisations, and internal 'structural' model parameters [19].

Figure 7 shows both histograms and smooth kernel density estimates (KDEs) for the same TODR input data as shown in Figure 5 and for the daily maximum temperatures.

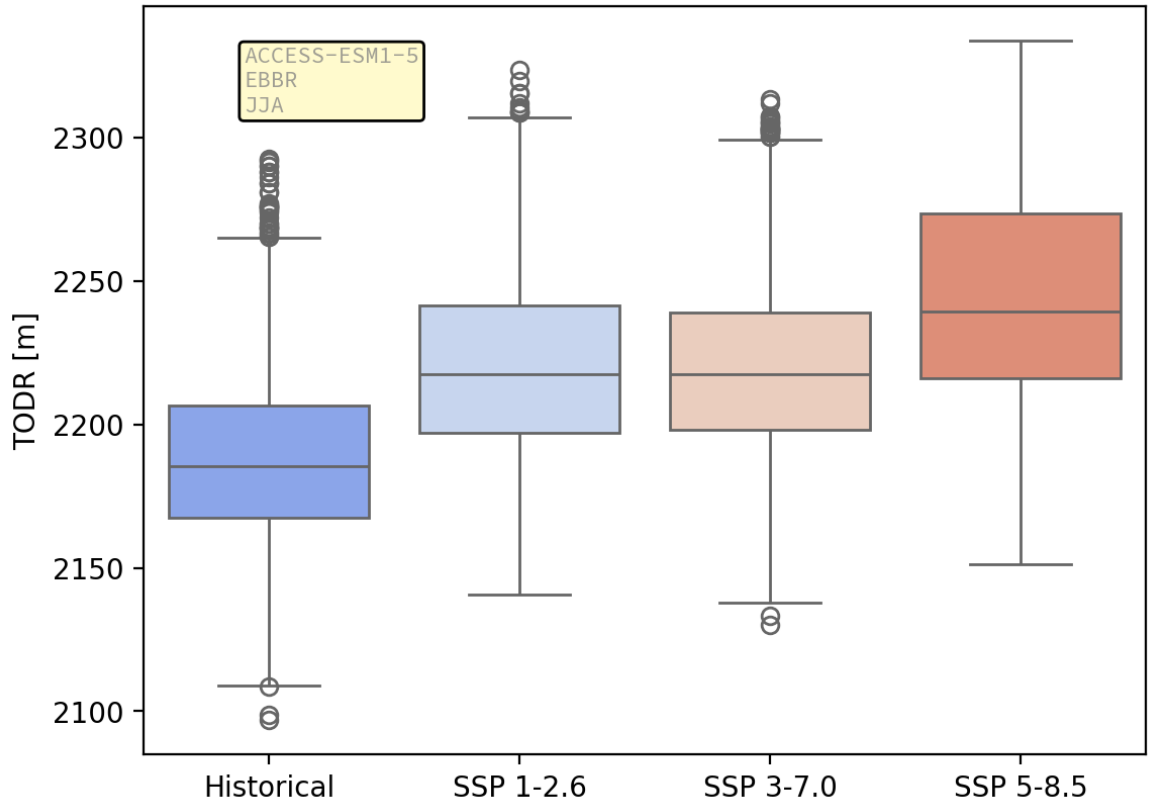

Figure 6. As for Figure 5 but for the ACCESS-ESM1-5 model and Brussels Airport (for JJA and a fully laden mass of 78,000 kg).

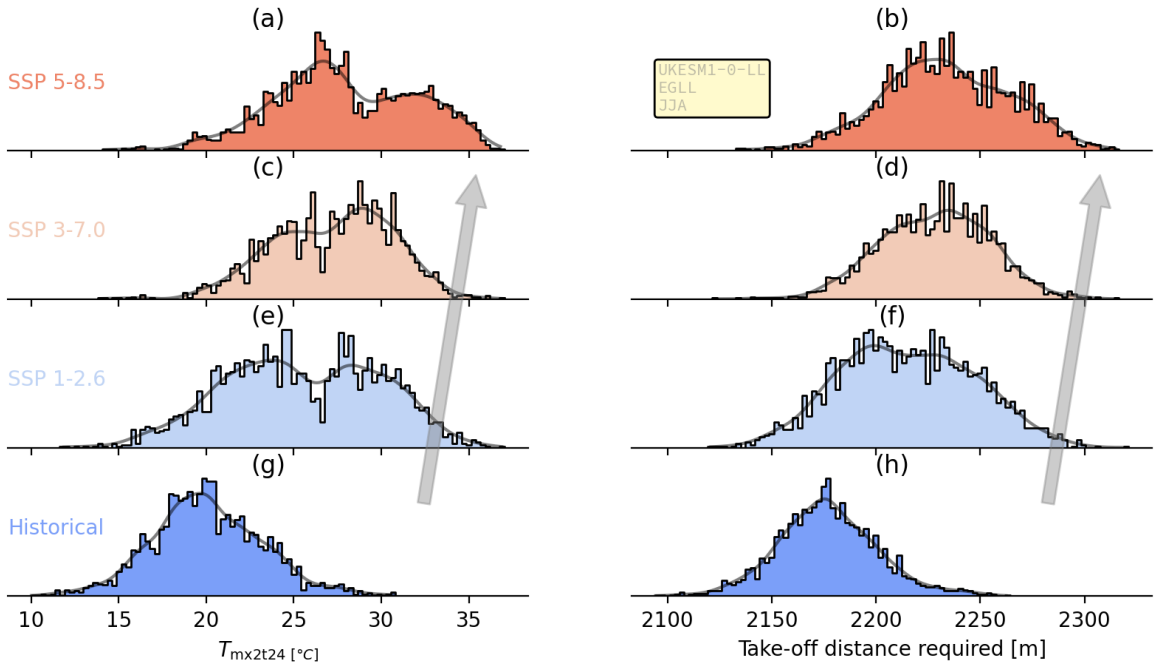

Figure 7. Normalised histograms (bars) kernel density estimation plots (lines) of TODR (**right**) and 24 h daily maximum temperature (**left**) for the historical period (**bottom**) and for increasing forcing, which increases in the vertical direction; historical (**g**,**h**), SSP1-2.6 (**e**,**f**), SSP3-7.0 (**c**,**d**), SSP5-8.5 (**a**,**b**). Data are for London Heathrow airport (ICAO code EGLL) in JJA using the UKESM1-0-LL climate model. The arrows are guides to the eye, indicating increased greenhouse gas forcing.

The correlation between the TODR and the daily maximum temperature is not one-to-one since the air pressure is also varying—see the discussion regarding Figure 8 below—but the overall link between the two variables shown in Figure 7 is clear. The increasing width of the distributions seen in Figure 7 is accompanied by a wider tail for the distributions on hotter days. The distributions in Figure 7 evolve from positively skewed unimodal distributions in the historical data to clearly bimodal ones in the future projection data, especially for temperature. This shift in distribution is in line with the already-changing European temperature distributions [20] and the increased occurrence of unusually hot days in particular Zhang et al. [21], which will lead to a decrease in the predictability of airport operations going forward. This feature, coupled with the general increase in overall temperatures with increased forcing, tends to make the TODR not only larger but also more variable.

To further emphasise the point that TODR does not have a one-to-one relationship with temperature, Figure 8 shows scatter plots of TODR and MTOM as a function of daily maximum temperature and pressure for Rome Ciampino airport. The co-variability is large; indeed, for a temperature of 20 °C, the variation in TODR simply due to pressure changes is approximately 50 m, and at 30 °C, these variations can account for MTOM changes of up to half a ton (500 kg, 1100 lb).

It is worth noting that the symbols for the MTOM are not shown when the calculated weight restriction is zero. What this means is that for temperatures below approximately 18 °C, the runway (2203 m for Rome Ciampino) is longer than the maximum TODR and weight restrictions are therefore not required.

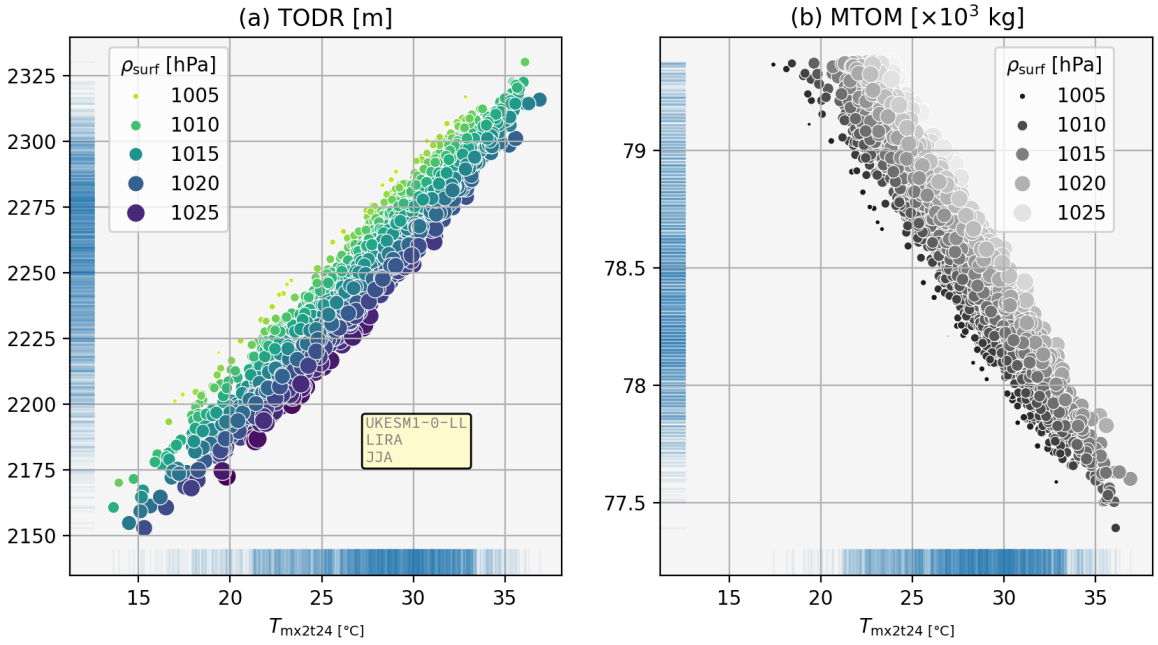

Figure 8. Take-off distance (**a**) and maximum take-off mass (**b**) as a function of the maximum temperature in the last 24 h, and (symbol size, colour/hue) surface air pressure for Rome Ciampino airport in JJA using the UKESM1-0-LL model. The short, blue lines attached to the axes show each data points that further illustrate the individual parameter values.

3.1.2. Ensemble

Figure 9 shows the model-ensemble spread of the probability of the 99th percentile of the historical distribution of TODR values being exceeded for the whole ensemble. The *y*-axis shows the number of days exceeding the 99th percentile of the historical distribution in each case. What this means is that a value of, say, 20, means an event that was historically a

1/100 day event, will occur 1/5th of the time in the future. Using a relative measure such as this alleviates the dependence on the results for different background temperatures in the sites studied.

Note that Figure 9 shows an inter-model spread of values for each model and site, whereas the other Figures illustrate the day-to-day variability of individual model/site pairs.

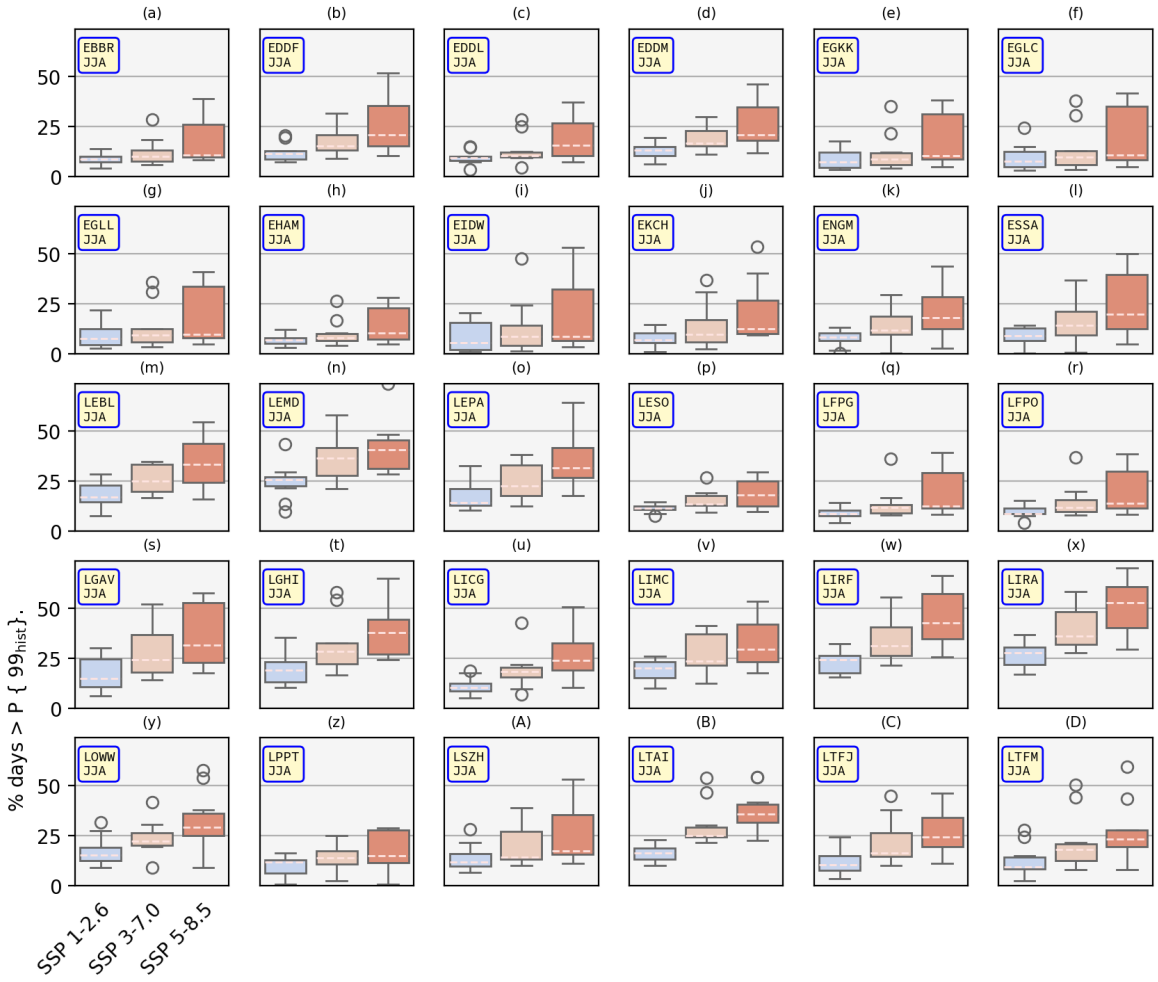

Figure 9. Ensemble spread of the probability of exceeding the 99th percentile of the historical distribution of TODR, JJA. Outliers (over 1.5 times the inter-quartile range of each distribution) are shown by circles. The maximum *y*-axis value is 1.05 times the highest value of any of the 'whiskers' shown. The individual subfigures (**a**–**z**,**A**–**D**) are for each airport considered and the ICAO codes for each site are shown in the top line of the respective inset boxes.

The spread of the results in Figure 9 varies considerably by airport and forcing scenario. This is especially evident for SSP5-8.5, which is partly a result of the larger spread of temperatures that results from the range of climate sensitivities in this subset of the CMIP6 model ensemble [22]. The larger spread in the temperatures, and hence TODRs, with the increased forcing seen in Figure 7 also contributes to the largest variability occurring in the fossil-fuelled development scenario, SSP5-8.5 in Figure 9.

Note that we are not explicitly considering the runway utilisation fraction (e.g., due to routine or event-based maintenance) in this work. However, this is important from an operational perspective since, for example, extreme heat is likely to degrade runway surfaces and hence affect maintenance logistics [23].

3.2. MTOM

The MTOM is obtained via an inversion of the TODR calculation, as detailed above; that is, the mass is calculated, which provides a TODR equal to the runway length at each airport. The aircraft will only be mass-limited if, at maximum loading, the TODR is greater than the runway length. Therefore, we only need to consider airports which have a TODR close to this value. Figure 10 shows the TODR at the maximum loading mass under the International Standard Atmosphere conditions in comparison to the runway lengths for the airports studied (shown numerically in Table A2). Note that, going forward, in this section we do not consider London City Airport, although its runway is short (1508 m), as it does not operate the A320 although it does use the shorter A319 and A318 variants.

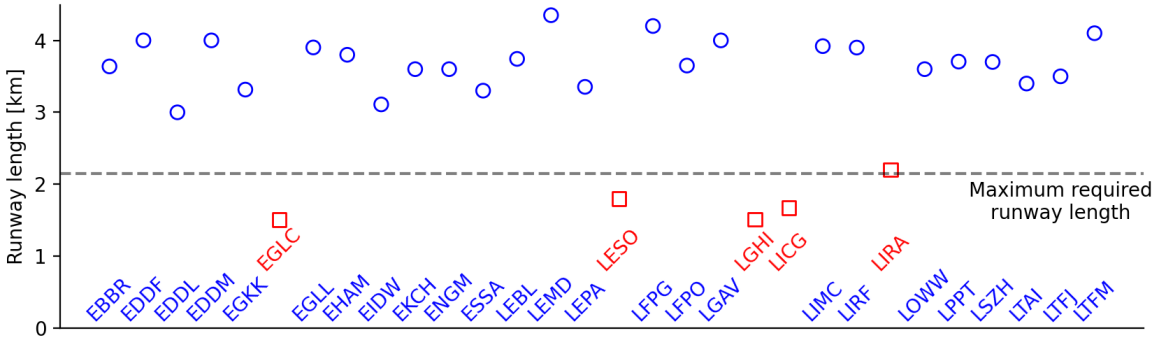

Figure 10. Runway lengths for each airport considered and the runway length calculated for the maximum-rated mass of the Airbus A320 using the International Standard Atmosphere. The airports that have runways shorter than or very close to the TODR for the maximum-rated mass are indicated in red and with raised ICAO codes. Those with longer runways, which will likely not be affected as temperatures increase, are indicated in blue.

Figure 11 shows projected changes in weight restrictions (in terms of the equivalent weight of passengers) over time for the four short-runway sites discussed above and the three future emissions scenarios compared to the respective historical mean values. Relative, as opposed to absolute values, are shown since this better enables a comparison of the changes to MTOW across sites in Figure 11. Analogous figures for a selection of American airports can be found in [5], and this study uses the same value for the average passenger's mass, i.e., 190 lb, or just over 86 kg, which includes carry-on baggage. Reducing passenger numbers is, of course, just one way of reducing payload, and we use passenger numbers as the 'unit' here to fit in with previous studies [4,5] and to avoid consideration of more subjective, and potentially operator-specific, factors such as hold baggage allowance, load factor, seat configuration, and fuel carriage. Future work would benefit from the inclusion of these factors.

Figure 11 shows that, even with the most optimistic future projections of greenhouse gas emissions (SSP1-2.6), our model indicates that the MTOM may have to be reduced by a weight equivalent to approximately five passengers per flight by the mid-2060s.

At the beginning of the future period considered, the MTOM is largely independent of the scenario used because, in 2035, the divergence in their emissions profiles is relatively small. Under SSP1-2.6, the stabilisation of emissions leads to broadly static reductions in MTOM of 5–6 passengers (or equivalent fuel or payload) over the whole period. This increases to ≈9 for SSP3-7.0 and as much as ≈13 for SSP5-8.5 by the end of 2064.

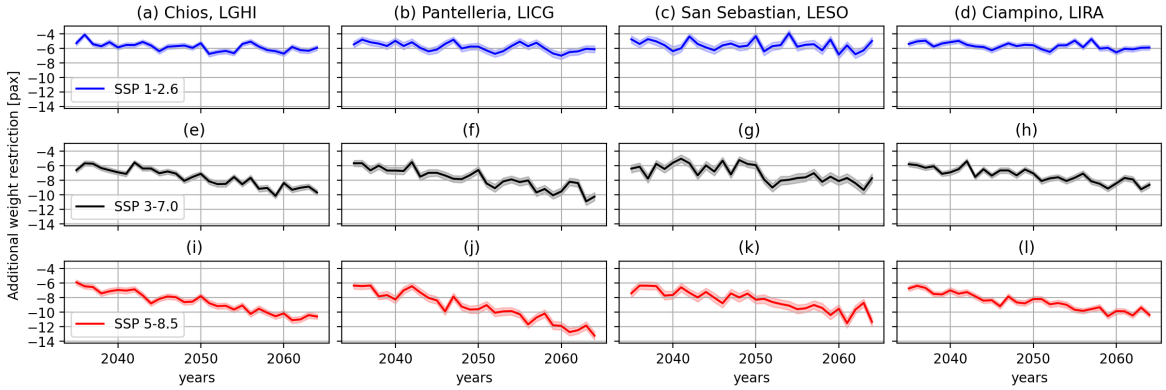

Figure 11. Additional weight restrictions in terms of number of passengers ('pax') relative to the respective historical value for four short-runway airports (**columns**) and three future emissions scenarios (**rows**). The sites considered are Chios (**a**,**e**,**i**), Pantelleria (**b**,**f**,**j**), San Sebastian (**c**,**g**,**k**) and Rome Ciampino (**d**,**h**,**l**) with the forcing increasing downwards.

To obtain an estimate for the increase in the frequency of weight-restriction days, it is important to note that—using manufacturer data under ISA conditions [4]—the TODR for a fully laden A320 is greater than any of the five short-runway sites considered here. In other words, even in the historical period, manufacturer data alone tell us that some level of payload restriction must apply, even at a conservatively cool (ISA) temperature of 15 °C, and even this excludes other deleterious factors, such as standing water and headwind.

Because of these 'built in' weight restrictions, to provide some tangible numbers we find the fraction of future days with weight restrictions at the 99th percentile of historical values for each short-runway site (analogous to the process followed above for TODR in Figure 9); this is shown in Figure 12.

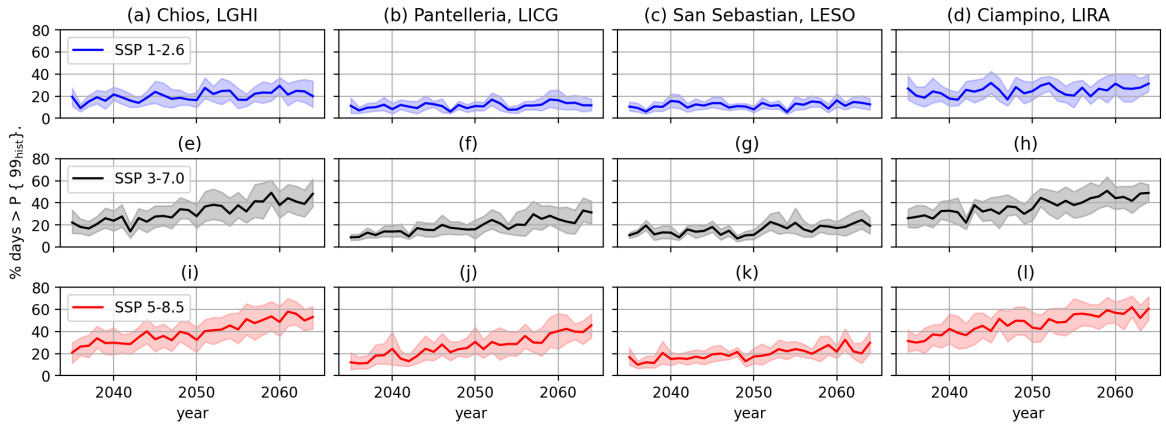

Figure 12. Number of days in which weight restrictions exceed the 99th percentile of historical values. The sites considered are Chios (**a**,**e**,**i**), Pantelleria (**b**,**f**,**j**), San Sebastian (**c**,**g**,**k**) and Rome Ciampino (**d**,**h**,**l**) with the forcing increasing downwards.

As in the top row of Figure 11, the values through time for SSP1-2.6 in Figure 12 are broadly static, reflecting the stabilisation of emissions in this scenario. However, unlike Figure 11, the number of days where MTOM $> P\{99_{\text{hist}}\}$ is highly dependent on the site with mean values as low as approximately 10% for Pantelleria and San Sebastian and as high as approximately 30% for Ciampino. For SSP3-7.0 and SSP5-8.5, we can see the same noticeable site-dependent variation in MTOM, plus the effect of the larger increases in temperature resulting from the increased emissions profiles.

The values—as for TODR in Figure 9—are striking. By definition, the historical equivalent value in Figure 12 is 1%, and so our data show that under a high future emissions

scenario, the days with conditions in which weight restrictions were required that occurred one day per hundred historically could occur up to 60 ± 10% of the time under an extreme future emissions scenario.

We now consider the probability distribution functions (PDFs) of all the weight restriction data for each period rather than over time. Figure 13 shows the model-ensemble mean of the normalised weight restriction PDFs of the periods considered relative to the historical mean. Subtracting this average provides a historical distribution with an integral of 0.5 either side of zero and more clearly shows the resulting increases in weight restrictions. Figure 14 displays equivalent plots but shows the variability (±1 standard deviation) of the model-ensemble mean rather than the mean. It also separates out the different scenarios to avoid regions with overlapping variability.

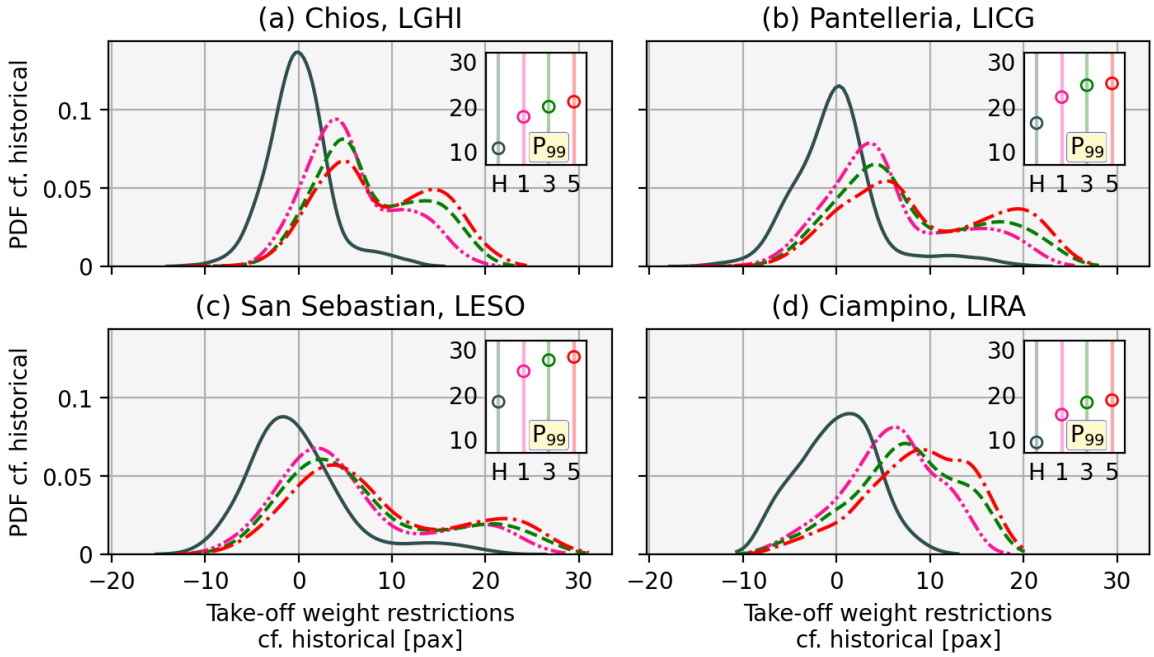

Figure 13. Probability density function of take-off weight restrictions relative to the historical value for each airport—Chios, Pantelleria, San Sebastian and Rome Ciampino—and emissions scenario (historical, dark grey; SSP1-2.6, pink; SSP3-7.0, green; SSP5-8.5, red). Negative values show restrictions below the respective historical mean, and hence the integral—i.e., the probability of occurrence—of the historical curve is symmetric at around zero. The smaller inset axes shows the 99th percentile values of the curves in the larger, main axes in terms of passenger equivalent weight for the historical ('H'), and future SSP forcings (1,3,5).

Again, as with the TODR distributions shown in Figure 7, there are two key features of the PDFs in Figures 13 and 14; the overall shape, and the changes to extreme values. In this analysis, we again consider the probability that the 99th percentile of historical values is exceeded. The historical distributions are broadly unimodal, albeit with small but non-negligible probabilities of high weight restrictions ('long tails'), particularly for San Sebastian, which has a 99th percentile value of the weight of almost 20 passengers above the historical mean. With increased greenhouse gas forcing, the shape of the PDFs tends to shift from unimodal to bimodal, again indicating an increase in the relative occurrence of extreme hot days. This is reflected in the increase in the 1/100 day weight restriction value, which (as shown in the insets in Figure 13), in each case, approximately doubles when comparing SSP5-8.5 values to the historical distribution.

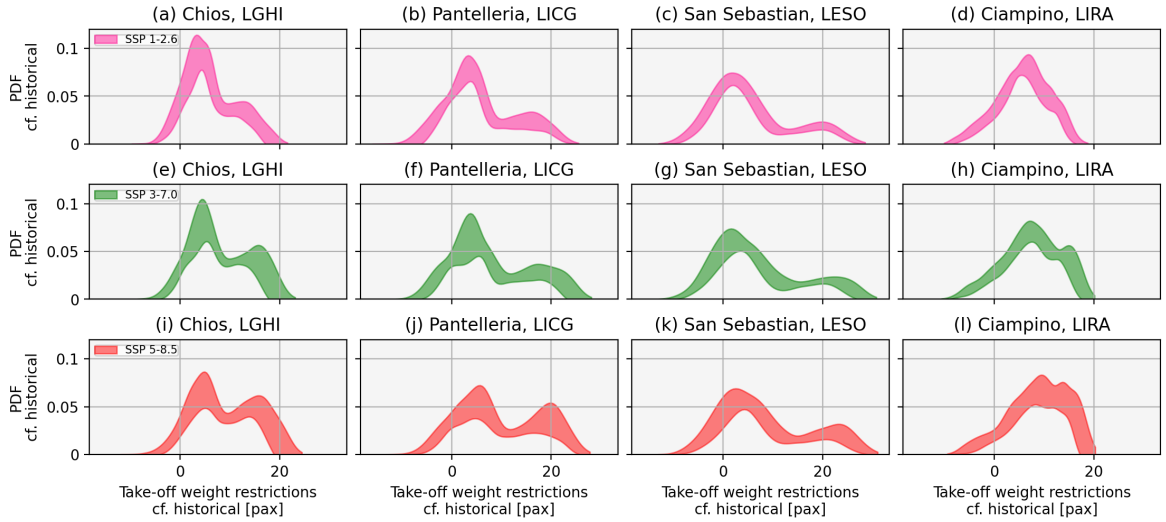

Figure 14. As in Figure 13 but showing the inter-model variability, ±1 standard deviation for Chios (**a**,**e**,**i**), Pantelleria (**b**,**f**,**j**), San Sebastian (**c**,**g**,**k**), and Ciampino (**d**,**h**,**l**).

4. Conclusions

Using a Newtonian force-balance model with open access input parameters, we examined how the take-off distance required (TODR) and maximum take-off mass (MTOM) may change in the future over European airspace. Ten state-of-the-art climate models were used to span a range of sensitivities of future temperature rises to increased greenhouse gas forcing, and the uncertainty in the emissions profiles themselves were quantified using three distinct Shared Socioeconomic Pathways, or SSPs.

Absolute projected changes in median TODR are small (approximately 50–110 m) with respect to the total runway length for many of the airports considered, several of which have runways which are over 4 km long. However, due to changes in the distribution of daily-maximum temperatures, occurrences of extreme (1/100 day) take-off distances, such as those in the recent past, may occur up to half the time by the mid-century. These changes may not adversely affect the ability of aircraft to safely operate within take-off distance limits; however, they are likely to have impacts on ground operations such as runway maintenance and utilisation, since some flights begin their acceleration at runway/taxiway intersections rather than at the runway extrema.

When an airport's available runway length is shorter than that required for a maximally laden aircraft, weight restrictions must be applied to reduce the take-off distance required. The resulting reduction in passenger numbers was quantified for four airports—Chios, Pantelleria, San Sebastian, and Rome Ciampino—showing projected reductions equivalent to approximately 5–12 passengers per flight by 2065 compared to the historical reference period. When the probability of exceeding the 99th percentile of historical values is considered as a function of time, following an SSP1-2.6 trajectory of emissions enables this quantity to stabilise between 10 and 20% (as does the passenger number restriction) but for higher-emissions futures, values of up to 60% are possible. The values of the 99th percentile weight restriction (again compared to the historical mean) could exceed 20 passengers equivalent in some cases; that is, more than 10% of the seats in an Airbus A320.

Future work in this project will consider other aircraft and engine types that are available in the openAP database; indeed, the current model has already been used for case studies of the Boeing 737 and Embraer 190. Future studies of widebody aircraft, such as the Airbus A380, would be a valuable extension to this work given their longer take-off distance requirements, i.e., they are already operating closer to the limits of available take-off performance than narrow-body aircraft such as the A320.

Thus far, we have employed pressure and temperature data in our calculations; however, humidity changes may also affect take-off performance. As yet, we have not considered these import effects, and there is some evidence (e.g., [24]) that changes to the amount of water vapour (and hence humidity) may have a non-negligible effect on air density, and therefore on TODR and MTOM. In addition, an increase in humidity will very likely affect passenger and ground crew comfort through changes to heat stress (e.g., [25]). A further—and crucial—meteorological factor is that of changing wind patterns affecting local 'true air speed'. Effects of this type were considered for a certain Greek airport in Gratton et al. [4], but to the authors' knowledge, a pan-European study of this kind has not been published. Indeed, since the input climate model data have global coverage, there is potential to incorporate an arbitrary number of sites into this framework by including site-extrapolation and/or bias correction into the performance model itself, as opposed to achieving this 'offline' for specific sites, as in this study.

Finally, work is also underway using the same study sites and models as used here to examine the effect of climate change on climb-rate-related safety parameters and noise pollution.

Author Contributions: Conceptualization, P.D.W.; methodology, P.D.W.; software, J.W., F.G. and M.V.; validation, J.W., F.G. and M.V.; formal analysis, J.W., F.G. and M.V.; investigation, J.W., P.D.W., F.G. and M.V.; resources, J.W., F.G. and M.V.; data curation, J.W., F.G. and M.V.; writing—original draft preparation, J.W.; writing—review and editing, J.W., P.D.W., F.G. and M.V.; visualization, J.W.; supervision, P.D.W.; project administration, P.D.W.; funding acquisition, P.D.W. All authors have read and agreed to the published version of the manuscript.

Funding: The research work for this article is part of the AEROPLANE project, which is supported by the SESAR 3 Joint Undertaking and its founding members, Grant Agreement ID 101114682, https://cordis.europa.eu/project/id/101114682, accessed on 18 December 2024.

Data Availability Statement: The raw data presented in the study are openly available in the Earth System grid Federation—ESGF—repository [26].

Acknowledgments: We thank the World Climate Research Programme (WCRP), which, through its Working Group on Coupled Modelling, coordinated and promoted CMIP6. We acknowledge the climate modelling groups for generating and making available their model output, the Earth System Grid Federation (ESGF) for archiving the data and providing access, and the many funding agencies who support the vital work of CMIP and the ESGF. We also acknowledge the computational services provided by the University of Reading's Academic Computing Cluster (RACC) and associated research software engineering staff.

Conflicts of Interest: The authors Federica Guerrini and Marco Venturini are employed by the Amigo s.r.l. The other authors declare no conflicits of interest.

Abbreviations

The following abbreviations are used in this manuscript:

TODR	Take-off Distance Required
MTOM	Maximum Take-off Mass
CMIP6	Coupled model Intercomparison Project, phase 6
ICAO	International Civil Aviation Organization code

Appendix A. ICAO Airport Codes and Runway Lengths

Tables A1 and A2 detail the airport sites studied.

Table A1. Airport ICAO codes.

Acronym	Description	Location
EBBR	Brussels Airport	Belgium
EDDF	Frankfurt am Main International Airport	Germany
EDDL	Dusseldorf International Airport	Germany
EDDM	Munich International Airport	Germany
EGKK	London Gatwick Airport	UK
EGLC	London City Airport	UK
EGLL	London Heathrow Airport	UK
EHAM	Amsterdam Airport Schiphol	Netherlands
EIDW	Dublin Airport	Ireland
EKCH	Copenhagen Kastrup Airport	Denmark
ENGM	Oslo Gardermoen Airport	Norway
ESSA	Stockholm-Arlanda Airport	Sweden
LEBL	Barcelona International Airport	Spain
LEMD	Madrid Barajas International Airport	Spain
LEPA	Palma De Mallorca Airport	Spain
LESO	San Sebastian Airport	Spain
LFPG	Charles de Gaulle International Airport	France
LFPO	Paris-Orly Airport	France
LGAV	Eleftherios Venizelos International Airport	Greece
LGHI	Chios Island National Airport	Greece
LICG	Pantelleria Airport	Italy
LIMC	Malpensa International Airport	Italy
LIRF	Leonardo Da Vinci (Fiumicino) International Airport	Italy
LIRA	Ciampino Airport	Italy
LOWW	Vienna International Airport	Austria
LPPT	Lisbon Portela Airport	Portugal
LSZH	Zurich Airport	Switzerland
LTAI	Antalya International Airport	Turkey
LTFJ	Sabiha Gokcen International Airport	Turkey
LTFM	Istanbul Airport	Turkey

Table A2. Runway lengths for all airports considered in this study in metres.

Airport Code	Runway Length (m)
EGLC	1508
LGHI	1511
LICG	1675
LESO	1800
LIRA	2203
EDDL	3000
EIDW	3110
ESSA	3301
EGKK	3316
LEPA	3354
LTAI	3400

Table A2. *Cont.*

Airport Code	Runway Length (m)
LTFJ	3500
EKCH	3600
ENGM	3600
LOWW	3600
EBBR	3638
LFPO	3650
LSZH	3700
LPPT	3705
LEBL	3743
EHAM	3800
LIRF	3900
EGLL	3902
LIMC	3920
EDDF	4000
EDDM	4000
LGAV	4000
LTFM	4100
LFPG	4200
LEMD	4350

Appendix B. Climate Models Used

Models are listed in Table A3. Further information on the CMIP6 ensemble can be found in [27] and all data is freely available from the Earth System Grid Federation, ESGF, https://esgf.llnl.gov/.

Table A3. Climate models used.

Model	Description
ACCESS-ESM1-5	CSIRO Commonwealth Scientific and Industrial Research Organisation, Australia [28]
CMCC-ESM2	CMCC Centro Euro Mediterraneo sui Cambiamenti Climatici, Italy [29]
CNRM-ESM2-1	CNRM Centre National de Recherches Météorologiques and CERFACS Centre Européen de Recherche et de Formation Avancée en Calcul Scientifique, France [30]
CanESM5	CCCMa Canadian Centre for Climate Modelling and Analysis, Canada [31]
EC-Earth3	EC-Earth Consortium Europe [32]
GFDL-ESM4	NOAA-GFDL National Oceanic and Atmospheric Administration, Geophysical Fluid Dynamics Laboratory, USA [33]
IPSL-CM6A-LR	IPSL Institut Pierre Simon Laplace, France [34]
MPI-ESM1-2-LR	MPI-M Max Planck Institute for Meteorology, Germany [35]
NorESM2-LM	NCC NorESM Climate Modelling Consortium, Norway [36]
UKESM1-0-LL	MOHC Met Office Hadley Centre, UK [37]

References

1. World Economic Forum. 2016. Available online: https://www.weforum.org/stories/2016/07/this-visualization-shows-you-24-hours-of-global-air-traffic-in-just-4-seconds/ (accessed on 25 November 2024).
2. EUROCONTROL. EUROCONTROL Aviation Outlook 2050. 2022. Available online: https://www.eurocontrol.int/publication/eurocontrol-aviation-outlook-2050 (accessed on 25 November 2024).

3. Gallardo, V.; Sánchez-Gómez, E.; Riber, E.; Boé, J.; Terray, L. Evolution of high-temperature extremes over the main Euro-Mediterranean airports. *Clim. Dyn.* **2023**, *61*, 1717–1740. [CrossRef]
4. Gratton, G.; Padhra, A.; Rapsomanikis, S.; Williams, P.D. The impacts of climate change on Greek airports. *Clim. Change* **2020**, *160*, 219–231. [CrossRef]
5. Coffel, E.; Horton, R. Climate Change and the Impact of Extreme Temperatures on Aviation. *Weather. Clim. Soc.* **2015**, *7*, 94–102. [CrossRef]
6. Coffel, E.D.; Thompson, T.R.; Horton, R.M. The impacts of rising temperatures on aircraft takeoff performance. *Clim. Change* **2017**, *144*, 381–388. [CrossRef]
7. Wang, K.; Peng, X.; Dan, B.; Liu, H.; Cheng, S.; Fu, N.; Fu, H.; Liu, C. Decreased Aircraft Takeoff Performance under Global Warming. *Atmosphere* **2023**, *14*, 106. [CrossRef]
8. Abram, N.; Gattuso, J.-P.; Prakash, A.; Cheng, L.; Chidichimo, M.P.; Crate, S.; Enomoto, H.; Garschagen, M.; Gruber, N.; Harper, S.; et al. IPCC Special Report on the Ocean and Cryosphere in a Changing Climate. In *The Ocean and Cryosphere in a Changing Climate*; Cambridge University Press: Cambridge, UK; New York, NY, USA, 2022; Chapter Framing and Context of the Report, pp. 73–130. [CrossRef]
9. Van Vuuren, D.P.; Stehfest, E.; Gernaat, D.E.; Doelman, J.C.; Van den Berg, M.; Harmsen, M.; de Boer, H.S.; Bouwman, L.F.; Daioglou, V.; Edelenbosch, O.Y.; et al. Energy, land-use and greenhouse gas emissions trajectories under a green growth paradigm. *Glob. Environ. Change* **2017**, *42*, 237–250. [CrossRef]
10. Fujimori, S.; Hasegawa, T.; Masui, T.; Takahashi, K.; Herran, D.S.; Dai, H.; Hijioka, Y.; Kainuma, M. SSP3: AIM implementation of shared socioeconomic pathways. *Glob. Environ. Change* **2017**, *42*, 268–283. [CrossRef]
11. Kriegler, E.; Bauer, N.; Popp, A.; Humpenöder, F.; Leimbach, M.; Strefler, J.; Baumstark, L.; Bodirsky, B.L.; Hilaire, J.; Klein, D.; et al. Fossil-fueled development (SSP5): An energy and resource intensive scenario for the 21st century. *Glob. Environ. Change* **2017**, *42*, 297–315. [CrossRef]
12. EUROCONTROL. *Performance Review Report 2019, an Assessment of Air Traffic Management in Europe During the Calendar Year 2019*; Technical report; Performance Review Commission: Brussels, Belgium, 2020.
13. Kang, X.; Zhao, G.; Song, H.; Zeng, X. Analysis of Density Altitude Characteristics at Chinese Airports. *Atmosphere* **2023**, *14*, 1784. [CrossRef]
14. Trentini, L.; Dal Gesso, S.; Venturini, M.; Guerrini, F.; Calmanti, S.; Petitta, M. A Novel Bias Correction Method for Extreme Events. *Climate* **2022**, *11*, 3. [CrossRef]
15. Trentini, L.; Venturini, M.; Guerrini, F.; Dal Gesso, S.; Calmanti, S.; Petitta, M. Identifying climate extremes in Southern Africa through advanced bias correction of climate projections. Accepted for publication in *Bull. Atmos. Sci. Technol.* **2025**. Available online: https://meetingorganizer.copernicus.org/EMS2024/EMS2024-604.html (accessed on 18 December 2024).
16. Sun, J.; Hoekstra, J.M.; Ellerbroek, J. OpenAP: An Open-Source Aircraft Performance Model for Air Transportation Studies and Simulations. *Aerospace* **2020**, *7*, 104. [CrossRef]
17. European Union Aviation Safety Agency. Easy Access Rules for Large Aeroplanes (CS-25). 2023. Available online: https://www.easa.europa.eu/en/document-library/easy-access-rules/easy-access-rules-large-aeroplanes-cs-25 (accessed on 18 December 2024).
18. Sun, J.; Ellerbroek, J.; Hoekstra, J.M. WRAP: An open-source kinematic aircraft performance model. *Transp. Res. Part C Emerg. Technol.* **2019**, *98*, 118–138. [CrossRef]
19. McNeall, D.; Williams, J.; Booth, B.; Betts, R.; Challenor, P.; Wiltshire, A.; Sexton, D. The impact of structural error on parameter constraint in a climate model. *Earth Syst. Dyn.* **2016**, *7*, 917–935. [CrossRef]
20. Stainforth, D.A.; Chapman, S.C.; Watkins, N.W. Mapping climate change in European temperature distributions. *Environ. Res. Lett.* **2013**, *8*, 034031. [CrossRef]
21. Zhang, Y.; Li, Q.; Ge, Y.; Du, X.; Wang, H. Growing prevalence of heat over cold extremes with overall milder extremes and multiple successive events. *Commun. Earth Environ.* **2022**, *3*, 73. [CrossRef]
22. Zelinka, M.D.; Myers, T.A.; McCoy, D.T.; Po-Chedley, S.; Caldwell, P.M.; Ceppi, P.; Klein, S.A.; Taylor, K.E. Causes of Higher Climate Sensitivity in CMIP6 Models. *Geophys. Res. Lett.* **2020**, *47*, e2019GL085782. [CrossRef]
23. Gratton, G.B.; Williams, P.D.; Padhra, A.; Rapsomanikis, S. Reviewing the impacts of climate change on air transport operations. *Aeronaut. J.* **2022**, *126*, 209–221. [CrossRef]
24. Yuan, W.; Dai, P.; Xu, M.; Song, W.; Zhang, P. Estimating the Impact of Global Warming on Aircraft Takeoff Performance in China. *Atmosphere* **2021**, *12*, 1472. [CrossRef]
25. Willett, K.M. HadISDH.extremes Part I: A Gridded Wet Bulb Temperature Extremes Index Product for Climate Monitoring. *Adv. Atmos. Sci.* **2023**, *40*, 1952–1967. [CrossRef]
26. Eyring, V.; Bony, S.; Meehl, G.A.; Senior, C.A.; Stevens, B.; Stouffer, R.J.; Taylor, K.E. Overview of the Coupled Model Intercomparison Project Phase 6 (CMIP6) experimental design and organization. *Geosci. Model Dev.* **2016**, *9*, 1937–1958. [CrossRef]

27. Gutiérrez, J.M.; Treguier, A.M.; Durack, P.J.; Emori, S.; Nowicki, S.; Ruiz, L.; Sierra, J.D.; Guilyardi, E.; Satoh, Y.; Stockhause, M. *Climate Change 2021: The Physical Science Basis*; Contribution of Working Group I to the Sixth Assessment Report of the Intergovernmental Panel on Climate Change; Cambridge University Press: Cambridge, UK; New York, NY, USA, 2023; Chapter AII—Annex II: Models, pp. 2087–2138. [CrossRef]
28. Ziehn, T.; Lenton, A.; Law, R.M.; Matear, R.J.; Chamberlain, M.A.; Ridgway, K.R.; Srbinovsky, J.; Stevens, L.; Vohralik, P.; Wang, Y.P. The Australian Earth System Model: ACCESS-ESM1.5. *J. South. Hemisph. Earth Syst. Sci.* **2020**, *70*, 1–28. [CrossRef]
29. Lovato, T.; Peano, D.; Butenschön, M.; Materia, S.; Iovino, D.; Scoccimarro, E.; Fogli, P.G.; Cherchi, A.; Bellucci, A.; Gualdi, S.; et al. CMIP6 simulations with the CMCC Earth System Model (CMCC-ESM2). *J. Adv. Model. Earth Syst.* **2022**, *14*, e2021MS002814. [CrossRef]
30. Séférian, R.; Nabat, P.; Michou, M.; Saint-Martin, D.; Voldoire, A.; Colin, J.; Decharme, B.; Delire, C.; Berthet, S.; Chevallier, M.; et al. Evaluation of CNRM Earth-System Model (CNRM-ESM2-1) for CMIP6. *J. Adv. Model. Earth Syst.* **2019**, *11*, 2530–2560. [CrossRef]
31. Swart, N.C.; Cole, J.N.S.; Kharin, V.V.; Lazare, M.; Scinocca, J.F.; Gillett, N.P.; Anstey, J.; Arora, V.; Christian, J.R.; Hanna, S.; et al. The Canadian Earth System Model version 5 (CanESM5.0.3). *Geosci. Model Dev.* **2019**, *12*, 4823–4873. [CrossRef]
32. Döscher, R.; Acosta, M.; Alessandri, A.; Anthoni, P.; Arsouze, T.; Bergman, T.; Bernardello, R.; Boussetta, S.; Caron, L.P.; Carver, G.; et al. The EC-Earth3 Earth system model for the Coupled Model Intercomparison Project 6. *Geosci. Model Dev.* **2022**, *15*, 2973–3020. [CrossRef]
33. Dunne, J.P.; Horowitz, L.W.; Adcroft, A.J.; Ginoux, P.; Held, I.M.; John, J.G.; Krasting, J.P.; Malyshev, S.; Naik, V.; Paulot, F.; et al. The GFDL Earth System Model version 4.1 (GFDL-ESM4.1): Model description and simulation characteristics. *J. Adv. Model. Earth Syst.* **2020**, *12*, e2019MS002008. [CrossRef]
34. Boucher, O.; Servonnat, J.; Albright, A.L.; Aumont, O.; Balkanski, Y.; Bastrikov, V.; Bekki, S.; Bonnet, R.; Bony, S.; Bopp, L.; et al. Presentation and evaluation of the IPSL-CM6A-LR climate model. *J. Adv. Model. Earth Syst.* **2020**, *12*, e2019MS002010. [CrossRef]
35. Mauritsen, T.; Bader, J.; Becker, T.; Behrens, J.; Bittner, M.; Brokopf, R.; Bunzel, F.; Esch, M.; Falk, D.; Fiedler, S.; et al. Developments in the MPI-M Earth System Model version 1.2 (MPI-ESM1.2) and its response to increasing CO2. *J. Adv. Model. Earth Syst.* **2019**, *11*, 998–1038. [CrossRef] [PubMed]
36. Bentsen, M.; Bethke, I.; Debernard, J.B.; Iversen, T.; Kirkevåg, A.; Seland, Ø.; Drange, H.; Roelandt, C.; Seierstad, I.A.; Hoose, C.; et al. The Norwegian Earth System Model, NorESM2—Evaluation of the CMIP6 DECK and historical simulations. *Geosci. Model Dev.* **2019**, *12*, 6165–6200. [CrossRef]
37. Sellar, A.A.; Jones, C.G.; Mulcahy, J.P.; Tang, Y.; Yool, A.; Wiltshire, A.; O'Connor, F.M.; Stringer, M.; Hill, R.; Palmieri, J.; et al. UKESM1: Description and evaluation of the UK Earth System Model. *J. Adv. Model. Earth Syst.* **2019**, *11*, 4513–4558. [CrossRef]